THE ASTROPHYSICAL JOURNAL, 492:754–760, 1998 January 10

ROSAT TIMING OF THE LMC PULSAR 0540−69[1]

STEPHEN S. EIKENBERRY,[2] GIOVANNI G. FAZIO, AND SCOTT M. RANSOM
Harvard-Smithsonian Center for Astrophysics, 60 Garden Street, Cambridge, MA 02138
Received 1997 June 19; accepted 1997 August 22

ABSTRACT

We present a timing study of the young rotation-powered pulsar 0540−69 in the Large Magellanic Cloud, based on 130 ks of archival *ROSAT* data spanning a ∼3 yr period. We use "$f-\dot{f}$" techniques to measure the pulsar frequency as a function of frequency derivative at 17 independent epochs. From these measurements we derive a timing solution with a braking index $n = 2.5^{+0.6}_{-0.7}$, and we compare this solution to previous timing studies of 0540−69. Using this frequency-based solution, we create 27 pulse profiles and perform a time-of-arrival (TOA) analysis to investigate further the pulsar's timing behavior. While we can fit smooth spin-down models to subsets of the TOAs spanning up to 2 yr successfully, we are unable to obtain acceptable phase-coherent fits to the entire 3 yr set of TOAs. This behavior provides the first clear evidence for timing noise in 0540−69. We discuss the implications of these results for understanding previous studies of the timing behavior of 0540−69.

Subject headings: pulsars: individual (PSR 0540−69) — stars: neutron — X-rays: stars

1. INTRODUCTION

The pulsar 0540−69 in the Large Magellanic Cloud (LMC) is one of the youngest and most luminous rotation-powered pulsars, with a spin-down age of $t_{sd} \sim 1500$ yr and a spin-down luminosity of $L_{sd} \sim 10^{38}$ ergs s^{-1}. The pulsar was first discovered as a 50 ms X-ray pulsar by Seward, Harnden, & Helfand (1984) using the *Einstein* IPC, with follow-up ground-based observations revealing optical pulsations of magnitude $m_V \sim 22.5$ (Middleditch & Pennypacker 1985). Despite the large spin-down luminosity of 0540−69 it is a faint radio pulsar, with a 640 MHz flux of only ∼0.4 mJy (Manchester et al. 1993), which requires long integrations with a 64 m telescope for detection. It is these observational properties of the pulsations that historically have made the timing of 0540−69 a difficult task: in the radio and optical regimes it requires large time allocations on large telescopes for extended periods. While X-ray observations can detect 0540−69 readily, the sheer scarcity of satellite time limits dedicated study in this band. Thus, many of the timing observations of 0540−69 have been conducted as "add-ons" to larger programs (such as X-ray and optical searches for a pulsar in SN 1987A).

Timing observations of 0540−69, in addition to being relatively scarce, have produced differing, often contradictory results. One of the most interesting measurements is of the pulsar braking index

$$n = \frac{f\ddot{f}}{(\dot{f})^2}, \tag{1}$$

where f is the pulsar frequency and $\dot{f}$ and $\ddot{f}$ are its first and second derivatives with respect to time. The braking index is a key indicator of the pulsar's magnetic field geometry and magnetospheric processes. The first reported measurement for 0540−69 was $n = 3.6 \pm 0.8$ by Middleditch, Pennypacker, & Burns (1987). Since then various groups have reported values of n ranging from 2.0 to 2.7, usually with small error bars excluding the results of other groups (see Table 1). Even when the braking indices agree, the frequency (and derivative) values differ so significantly that such agreement is likely a coincidence (see, e.g., Nagase et al. 1990; Manchester & Peterson 1989). Furthermore, in order to explain these discrepancies, virtually every paper listed in Table 1 has claimed that the results prior to its own were contaminated by glitches, or at least that a glitch occurred between the observations. Thus the timing behavior of 0540−69 is hardly a settled matter, more than a decade after the pulsar's discovery.

In this paper, we present a new timing analysis of 0540−69 by utilizing a unique and previously untapped resource for this work: the *ROSAT* data archive. Due to the wide field of the *ROSAT* PSPC (∼1° radius), 0540−69 is in the field of view for a large fraction of the pointings toward the LMC (see Fig. 1). Because there was a large number of programs studying a wide range of objects in the LMC (i.e., LMC X-1, SN 1987A, supernova remnants, etc.), the total time during which 0540−69 was in the PSPC field comes to nearly 160,000 s. Previously, most of these data have been difficult to use for timing of 0540−69 due to the nature of scheduling X-ray observations; typically the pulsar was observed for several hundred seconds at a time, with gaps of hours, days, or even weeks until the next pointing. Over such long time spans the effects of the pulsar's $\dot{f}$ become very important, and traditional methods (e.g., fast-Fourier transforms [FFTs]) are inadequate for performing the timing analysis over these gaps. However, the individual small exposures alone often do not produce sufficient signal-to-noise for timing analysis. Thus, for this work we employ more advanced "$f-\dot{f}$" techniques (Ransom & Eikenberry 1997; Eikenberry 1997) to determine the Fourier power as a function not only of frequency f, but also of the frequency derivative $\dot{f}$, that is, $P(f, \dot{f})$. Such techniques are suitable for pulsar timing with "gappy" data, and thus allow us to analyze the unique *ROSAT* PSPC archival data set for timing of 0540−69.

In the following sections, we first discuss the archival X-ray observations from *ROSAT* and the data reduction techniques used to determine the pulsar's Fourier power spectrum for each observation, $P(f, \dot{f})$. Next, we present

[1] This research has made use of data obtained from the High Energy Astrophysics Science Archive Center (HEASARC) provided by NASA's Goddard Space Flight Center.

[2] Current address: Downs Laboratory, 320-47, California Institute of Technology, Pasadena, CA 91125.

TABLE 1

PREVIOUSLY DETERMINED BRAKING INDICES

Braking Index (n)	Time Span (MJD)	Authors
3.6 ± 0.8	44,186–46,112	1
2.01 ± 0.02	46,600–47,400	2
2.74 ± 0.10	45,924–46,246	3
2.02 ± 0.01	46,900–47,500	4
2.04 ± 0.02	47,540–48,360	5
2.080 ± 0.003	46,110–47,725	6

REFERENCES.—(1) Middleditch et al. 1987; (2) Manchester & Peterson 1989; (3) Ögelman & Hasinger 1990; (4) Nagase et al. 1990; (5) Gouiffes et al. 1992; (6) Deeter et al. 1997.

the pulsar timing solution as determined by the analysis of the various $P(f, \dot{f})$ measurements, and we compare this solution to several previous determinations. We then move on to a refined timing solution using pulse time-of-arrival (TOA) analyses. Next, we discuss the implications of these results for understanding the timing behavior of 0540−69 in the context of prior work. Finally, we present our conclusions.

2. OBSERVATIONS AND DATA REDUCTION

We selected the archival data for this work using the World Wide Web based archival search software of the HEASARC project at NASA Goddard Space Flight Center. Having determined empirically that the deterioration of the PSPC point-spread function (PSF) for radii greater than 30′ resulted in unacceptably low signal-to-noise ratios, we chose data sequences for which 0540−69 was within a 30′ radius of the field center. We also selected only those sequences that had total on-source exposure times of $t_{obs} > 2500$ s, as shorter total exposures usually resulted in individual exposures too short to be useful. We list the selected data sequences in Table 2.

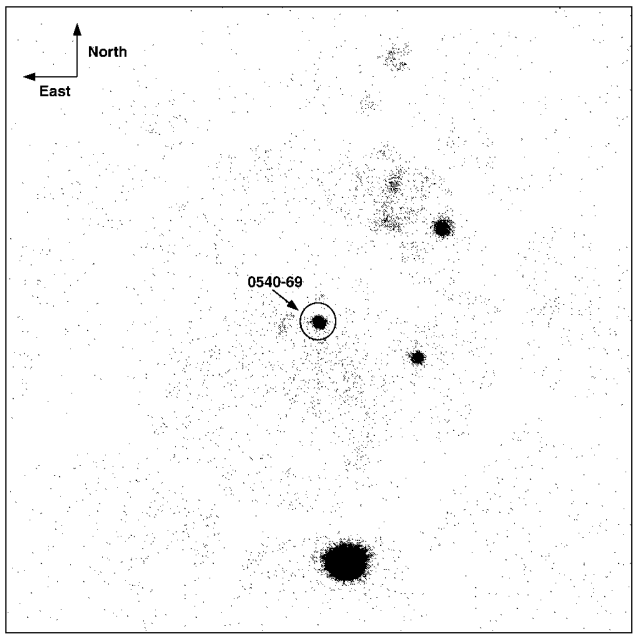

FIG. 1.—Typical *ROSAT* PSPC image of the Large Magellanic Cloud. The source at the field center is 0540−69. LMC X-1 is the bright source at the bottom of the field.

TABLE 2

LIST OF *ROSAT* DATA SEQUENCES

Sequence	MJD Start	MJD End	Total Exposure (s)
WP110167	48,059	48,059	2966
WP150044	48,090	48,136	5333
RH150008[a]	48,097	48,098	18,126
WP400052	48,307	48,310	8953
WP600100	48,367	48,726	24,989
RP500100	48,535	48,756	27,207
RP400079	48,589	49,135	7666
RP500131	48,741	48,760	16,069
RP500140A1	49,084	49,087	9993
RP500140A2	49,158	49,173	10,766

[a] This sequence used the *ROSAT* HRI instrument.

We used the PROS software package within IRAF to create images of the field (see Fig. 1 for an example) and to select all the photon events within a circular aperture centered on 0540−69, varying the aperture radius depending on the pulsar PSF in each observation. We then created time-sorted event lists and light curves for each sequence. For easier processing, we subdivided the sequences into "pieces" with maximum durations of $t_{obs} < 2$ weeks (see Table 3 for a listing). We then corrected the photon event times to the solar system barycenter using a pulsar position of R.A. = $05^h40^m11^s.03$ and decl. = $-69°19'57''.5$ (J2000)[3] (Gouiffes, Finley, & Ögelman 1992, hereafter GFÖ), and we exported these photon arrival times outside IRAF for the pulsation analysis.

We calculated the pulsar Fourier power spectrum for each piece in Table 3 using the signal-folding technique for $f-\dot{f}$ analysis (Ransom & Eikenberry 1997; Eikenberry 1997; Eikenberry et al. 1997). Since this technique has been described elsewhere, we only briefly summarize it here. The effect of a frequency derivative or a frequency offset between the Fourier frequency and the pulsar frequency is negligible over a small time interval, but it can have a significant impact on the resulting Fourier power over an entire time series. Thus, we subdivide the pulsar time series into seg-

TABLE 3

LIST OF *ROSAT* DATA PIECES

Piece ID	MJD Start	MJD End
WP110167	48,059	48,059
WP150044 a–f	48,090	48,091
RH150008	48,097	48,098
WP400052	48,307	48,310
WP600100 a–b	48,367	48,371
RP500100 a	48,535	48,535
RP400079 b–d	48,635	48,635
WP600100 f–j	48,703	48,710
WP600100 k–n	48,712	48,718
WP600100 o–p	48,723	48,726
RP500131 a–c	48,741	48,741
RP500100 b	48,742	48,742
RP500100 c–f	48,752	48,756
RP500131 d–s	48,753	48,760
RP500140A1	49,084	49,087
RP500140A2 a–f	49,158	49,165
RP500140A2 g–j	49,171	49,173

[3] Deeter, Nagase, & Boynton (1997) use a different position for the pulsar, offset by ∼4″. While this offset is significant for the TOA analysis (as we discuss in the next section), it does not affect the frequency results here and in § 3.1 significantly.

ments of length ~ 4 s and calculate the Fourier transform over each segment, F_i. The FFT algorithm gives a Fourier amplitude equal to the complex sum of the F_i. A frequency derivative or frequency offset will cause each F_i to suffer a phase shift relative to its neighbors, so that when added they are slightly out of phase, the F_i vectors are rotated in the complex plane, and power is lost. However, this effect can be countered by "derotating" the F_i through multiplication by a complex phase factor corresponding to the effect of the frequency derivative and offset, so that the resulting $F_i^{(\mathrm{rot})}$ will add in phase, and power will be recovered. Therefore, for a given frequency offset $w = f - f_0$ and a given frequency derivative $\dot{f}$, we multiply the F_i by the phase factors

$$e^{-i\phi_i}, \quad \phi_i = wt_i + \tfrac{1}{2}\dot{f}t_i^2, \tag{2}$$

where t_i is the time elapsed from the beginning of the observation to the ith segment.

We selected an initial frequency for signal folding by taking a small segment of data, performing an FFT on it, and taking the frequency from the largest Fourier peak near $f \sim 19.85$ Hz. We then "folded" the time series at this initial guess frequency, saving the complex Fourier amplitudes for every 4.096 s segment of the time series. Next we "derotated" this Fourier series for a range of frequency and frequency-derivative combinations and calculated the Fourier power at each combination, $P(f, \dot{f})$. We varied the range and step size for f according to the duration of the data piece, but we used a uniform set of $\dot{f}$ values from -1.9×10^{-10} to -1.85×10^{-10} Hz s^{-1} with a step size of $\Delta\dot{f} = 1 \times 10^{-14}$ Hz s^{-1}. We repeated these steps for the next four higher harmonics of the fundamental frequency and added the resulting powers to obtain the sum power, $P_{\mathrm{sum}}(f, \dot{f})$. Finally, using $\sigma_P = (2P)^{1/2}$ for the jth piece at each value of $\dot{f}$, we calculated the best-fit initial frequency $f_{0,j}(\dot{f})$ and the frequency uncertainty $\sigma_f(\dot{f})$.[4]

3. TIMING ANALYSIS

3.1. *Frequency-based Timing Solution*

Once we had the starting time for the data pieces and their frequency estimates $f_{0,j}(\dot{f})$, we calculated a timing solution for the pulsar of the form

$$f(t) = f_0 + \dot{f}t + \tfrac{1}{2}\ddot{f}t^2 . \tag{3}$$

To do so, we looped over a range of $\ddot{f}$ and the $\dot{f}$ values above, calculating the least-squares value of f_0 (the pulsar frequency at the beginning of the first data piece, MJD 48,059.7864091) for the data, and the corresponding value of χ^2. We found a minimum χ^2 value of 1.9 for 15 degrees of freedom (or $\chi_\nu^2 = 0.13$)[5] for the parameters listed in Table 4.

We compare this timing solution to those of previous works in Figure 2. We find excellent agreement between our solution and the ephemeris of Deeter et al. (1997, hereafter DNB). We see a significant discrepancy with the ephemeris of GFÖ; the difference between their ephemeris and our local frequency measurements results in $\chi^2 = 1422$ for 17 degrees of freedom (dof). We find very large discrepancies between our solution and the extrapolation of the timing ephemerides of Ögelman & Hasinger (1990) and Manchester & Peterson (1989).

TABLE 4

FREQUENCY-BASED TIMING SOLUTION

Parameter (1)	Value[a] (2)
Epoch (MJD)	48,059.78640911
f_0 (Hz)	19.8534877(18)
$\dot{f}_0$ (Hz s^{-1})	$-1.8886(8) \times 10^{-10}$
$\ddot{f}$ (Hz s^{-2})	$4.5^{+1.2}_{-1.4} \times 10^{-21}$
Braking index (n)	$2.5^{+0.6}_{-0.7}$

[a] Values in parentheses in col. (2) are the uncertainties in the last quoted digits.

3.2. *TOA-based Timing Solutions*

3.2.1. *TOA Determination*

We next moved to a time-of-arrival (TOA) timing analysis for pulsar 0540−69 in order to refine the timing solution above. TOA analysis links the individual observations in phase, providing a much more sensitive probe of the pulsar's timing behavior. In order to carry out this analysis, we first created pulse profiles. For added timing sensitivity, we subdivided some of the data pieces, resulting in a total of 27 pulse profiles.[6] We folded the pulse profiles using the timing solution in Table 4, with 1 ms phase bins.

We next created a master pulse profile as follows. First, we correlated the first pulse profile against the second, shifting the second profile bin-by-bin to obtain the correlation coefficient as a function of phase shift. We then added the shifted second profile to the first profile at the phase shift that produced the largest correlation coefficient. We then correlated the sum profile against the third profile, adding the shifted third profile to the sum as we did for the second profile, and we repeated this procedure for the fourth through 27th profiles. This resulted in a temporary master profile. However, in creating this temporary master, each profile was correlated against a different sum profile from all the other profiles, leaving room for systematic errors. In order to remove these potential errors, we created the final master pulse profile by correlating all of the individual profiles against the temporary master, shifting each bin-by-bin, and adding all the shifted profiles using the shifts that produce the largest correlation coefficient with the temporary master profile. We show the resulting master pulse profile in Figure 3. We also compared the individual pulse profiles to the master profile in order to search for long-term changes in the pulse shape. We found no significant evidence of such variability.

We next determined the individual pulse TOAs as follows. Taking the phase as the bin shift that produced the largest correlation coefficient, we determined the pulse phases by correlating the profiles against the master pulse profile in Figure 3. We determined the uncertainties in the

[4] For signals with window functions sufficiently close to a simple square window, the frequency can be determined with an uncertainty smaller than this by a factor of $\sim$2–3 for 0540−69 (see Ransom & Eikenberry 1997; Eikenberry 1997). However, for several pieces here, the window function is sufficiently different that this is not true. Thus for the sake of consistency we use this estimate for σ_f, although we know that it is an overestimate in several cases. Note also that the effects of the frequency second derivative $\ddot{f}$ on $f_{0,j}(\dot{f})$ are negligible over the maximum duration of each individual piece.

[5] Note that the procedure above may overestimate σ_f by a factor of up to 2–3, resulting in a correspondingly low value of χ_ν^2.

[6] We excluded the HRI data sequence RH150008, as the different energy response of the HRI may produce systematic differences in the observed pulse shape and thus systematic phase offsets for this analysis.

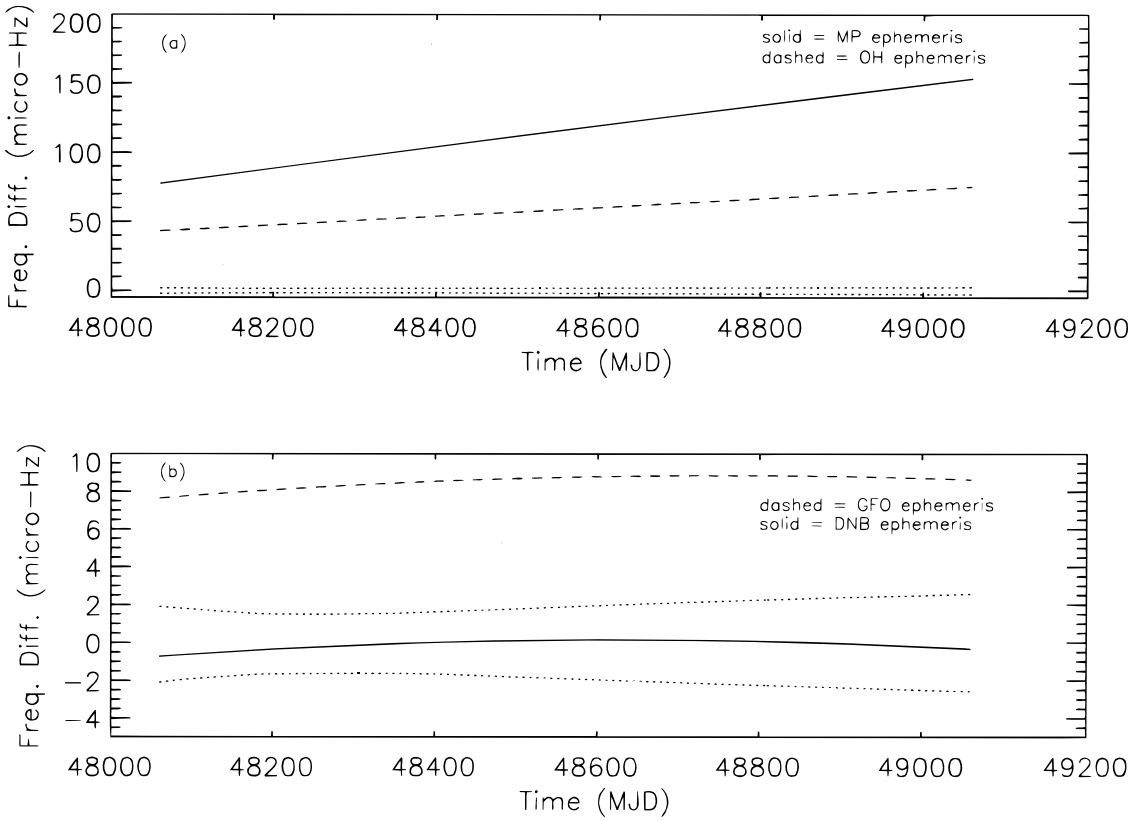

FIG. 2.—Frequency difference between our frequency-based timing solution in Table 4 and other published ephemerides for 0540−69 (*a*) Manchester & Peterson (1989) and Ögelman & Hasinger (1990) ephemerides. (*b*) GFO and DNB ephemerides. The dotted lines bound the $\pm 1\ \sigma$ range in allowed frequency for our solution.

phases (and thus in the TOAs) by a Monte Carlo simulation. First, we assumed that the errors in the pulse profiles were dominated by the Poissonian uncertainties in the number of events in each phase bin. For a given pulse profile, we added to each phase bin a random number drawn from a distribution corresponding to the uncertainty in the number of events in the phase bin, resulting in a simulated pulse profile. We then correlated this simulated profile against the master profile, giving the simulated pulse phase. We repeated this procedure 1000 times, taking the uncertainty in the pulse phase to be the standard deviation in the simulated pulse profiles plus the systematic uncertainty of ± 0.5 phase bins. The pulse TOA is then the start time of the observation plus the pulse phase multiplied by the pulsar period.

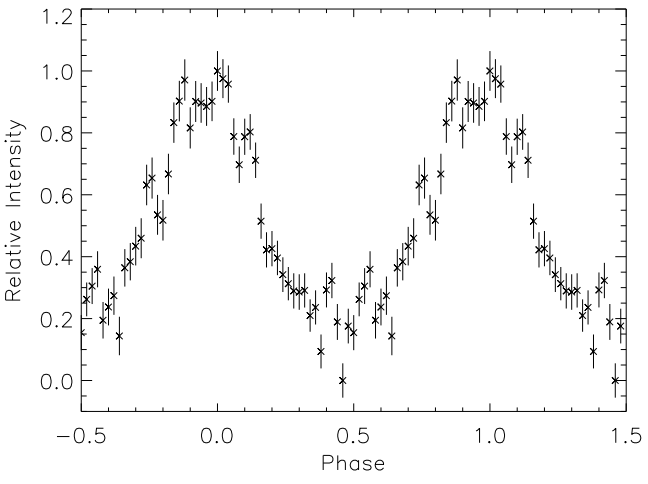

FIG. 3.—*ROSAT* PSPC master pulse profile for 0540−69

3.2.2. *Timing Solutions I*

In order to determine the timing solution given the pulse TOAs, we simply calculated the χ^2 for the phase residuals to a solution of the form

$$\phi(t) = \phi_0 + f_0 t + \tfrac{1}{2}\dot{f}_0 t^2 + \tfrac{1}{6}\ddot{f} t^3 \ . \quad (4)$$

We resorted to an iterative process in order to calculate the χ^2 values over the entire range of parameter space. First, we selected a segment of our time span that is particularly dense with TOA determinations, which covers TOAs 13–23. We then looped over the range of allowed solutions from Table 4 using the step sizes (df_0, $d\dot{f}_0$, $d\ddot{f}$) dictated by the $\sim 5 \times 10^6$ s time span of this subset of our observations. We then expanded the subset to include TOAs 10–23, looping over the allowed solutions from the 13–23 subset with smaller step sizes corresponding to the time span of the 10–23 data set. We repeated this procedure for the TOA 1–23 subset, and finally the TOA 1–27 subset.

For the subset of TOAs 1–23, we found two different timing solutions, A and B in Table 5, both with $\chi^2 \simeq 19$ for 19 degrees of freedom. The difference in these solutions is due to ambiguities in the pulse cycle count over some of the large gaps in the *ROSAT* coverage of 0540−69. Note that the χ^2 values for both solutions are very good. However, when we extended the analysis to the full set of TOAs, we found $\chi^2_{\rm min} = 39.3$ for 23 degrees of freedom, a significantly poorer fit (see Figure 4).

TABLE 5

TOA-BASED TIMING SOLUTIONS

	PARAMETERS[a]					
SOLUTION	$f_0 - f_{ref}$[b] (10^{-9} Hz)	$\dot{f}_0$ (10^{-10} Hz s^{-1})	$\ddot{f}$ (10^{-21} Hz s^{-2})	BRAKING INDEX	TOA RANGE	POSITION[c]
A.....	6456 (10)	−1.888147 (9)	3.67 (3)	2.05 (2)	1–23	1
B.....	6972 (10)	−1.888279 (8)	3.88 (3)	2.16 (2)	1–23	1
C.....	5580 (15)	−1.88771 (5)	2.930 (5)	1.632 (3)	10–27	1
D	6750 (20)	−1.888231 (7)	3.855 (11)	2.147 (6)	10–27	1
E.....	8872 (12)	−1.8891 (2)	4.998 (7)	2.781 (4)	10–27	1
F.....	9260 (50)	−1.889071 (17)	5.24 (3)	2.92 (2)	10–27	1
G	6547 (10)	−1.888187 (9)	3.84 (3)	2.14 (2)	1–23	2
H	6644 (5)	−1.888235 (5)	3.955 (16)	2.202 (9)	1–23	2
I.....	8900 (1100)	−1.88886 (19)	4.762 (11)	2.650 (6)	1–23	2
J	5280 (30)	−1.887672 (7)	2.809 (16)	1.565 (9)	10–27	2
K	6100 (50)	−1.888016 (17)	3.52 (3)	1.96 (2)	10–27	2
L.....	6490 (40)	−1.888156 (15)	3.76 (2)	2.094 (11)	10–27	2
M	8400 (1100)	−1.88869 (20)	4.470 (17)	2.488 (9)	10–27	2
N	10192 (12)	−1.889163 (5)	5.041(8)	2.804 (4)	10–27	2
O	7286 (5)	−1.888489 (3)	4.450 (5)	2.477 (3)	1–27	2

[a] Values in parentheses are the uncertainties in the last quoted digits. Pos = 1 solutions are referenced to MJD 48,059.78640911. Pos = 2 solutions are referenced to MJD 48,059.78640904.

[b] $f_{ref} = 19.85348$ Hz.

[c] Pulsar position used: (1) GFÖ, (2) DNB.

This poorer fit initially suggested the presence of a glitch between TOAs 23 and 24, so we repeated the determination of a timing solution starting from TOAs 10–23 and extending the subset to TOAs 10–27. We found a family of four solutions with $\chi^2_{min} = 16.8$ for 14 degrees of freedom (solutions C–F in Table 5), showing that it is possible to fit a model of the form of equation 4 over this time span.[7] While this does not preclude the presence of a glitch between TOAs 23 and 24, it does make it impossible to determine conclusively that a glitch did occur. However, when we extend solutions C–F to the full set of TOAs, we again find a poor fit ($\chi^2_{min} = 39.4$ for 23 dof).

[7] Again, the differences in solutions C–F in Table 5 are due to pulse numbering ambiguities over the larger gaps in the *ROSAT* coverage of 0540−69.

3.2.3. *Timing Solutions II*

The above analysis assumed a position for 0540−69 determined by X-ray imaging observations. However, DNB have suggested recently that a more accurate position for the pulsar is R.A. = $5^h40^m11^s.57$, decl. = −69°19′54″.9 (J2000), as determined by timing observations. This ∼4″ shift in position will cause a systematic shift in the observed barycentric TOAs consisting of a sine wave with a 1 yr

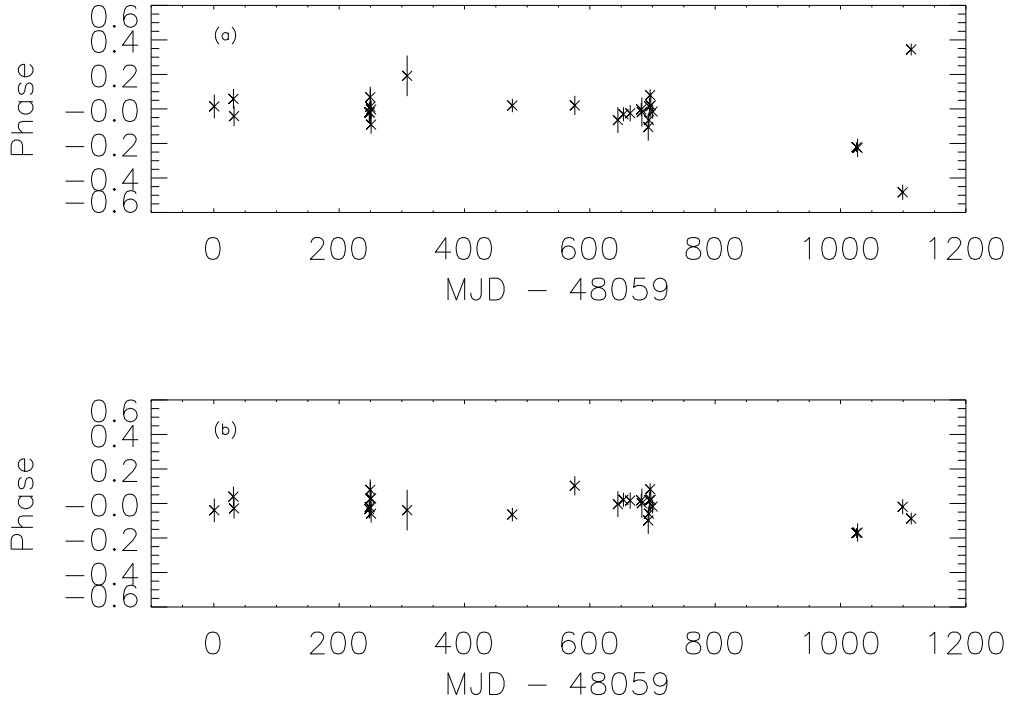

FIG. 4.—Phase residuals for (*a*) solution A in Table 5, and (*b*) solution B in Table 5. While both solutions give $\chi^2 \sim 19$ for TOAs 1–23, they have $\chi^2 = 321$ and 74 for all 27 TOAs.

period and an amplitude of ∼10 ms, significant variations given our typical TOA uncertainties of ∼2–4 ms. (Note that such a sine wave would produce systematic frequency offsets $\delta f < 2 \times 10^{-9}$ Hz, much less than the statistical uncertainties in the individual frequencies used for the solution in Table 4.) In order to check whether these effects were responsible for the poor fits seen above, we calculated a revised set of TOAs using the position of DNB.

We then repeated the timing analysis as above for the revised TOAs. For the subset of TOAs 1–23, we found a family of three solutions with $\chi^2_{\rm min} = 18.6$ for 19 dof (solutions G–I in Table 5), again an excellent fit. However, when we extended these solutions to the full set of revised TOAs, we again found a much poorer fit $\chi^2_{\rm min} = 44.5$ for 23 dof. For the subset of TOAs 10–27, we also found five acceptable solutions (J–N in Table 5) with $\chi^2_{\rm min} = 14.3$ for 14 dof. When we extended these solutions to TOAs 1–27 we found a solution with $\chi^2 = 32.1$ for 23 degrees of freedom (solution O in Table 5). While this solution is better than those we found previously, we note that χ^2 increased by $\Delta\chi^2 = 17.8$ for TOAs 1–9. Thus, while TOAs 10–27 may follow this solution, we can reject the hypothesis that the first 9 TOAs follow the same solution at the 95% confidence level.

4. DISCUSSION

4.1. *Frequency-determined Solutions*

As we saw in Figure 2, our frequency-determined solution in Table 4 provides an acceptable match with the ephemeris of DNB, and also with that of Nagase et al. (1990). DNB's paper is a continuation of the Nagase et al. (1990) work by several of the same authors, and expands the *Ginga*-based X-ray timing of Nagase et al. (1990) to include more *Ginga* data along with optical data and a small amount of previously published *ROSAT* data (Finley et al. 1993). The fact that our independent timing solutions agree to such high accuracy implies that they do indeed represent the frequency behavior of 0540−69.

We find a significant discrepancy between the solution in Table 4 and the timing ephemeris of GFÖ. GFÖ noticed a similar mismatch with the ephemeris of Nagase et al. (1990), and hypothesized that this discrepancy might be due to a third derivative of the frequency with time, combined with the fact that the Nagase et al. (1990) observations had an earlier average epoch than GFÖ. However, the fact that we match the *Ginga* ephemeris at an even later epoch seems to contradict this assessment. When we compare our frequency-determined solution to the local frequency measurements of GFÖ, we find excellent agreement (though the typical uncertainties in the GFÖ measurements are larger than the discrepancy seen in Figure 2). Thus, the discrepancy seems to arise in the TOA-based solution for the GFÖ data.

In comparing our frequency-based timing solution to the ephemerides of Manchester & Peterson (1989) and Ögelman & Hasinger (1990), we find very large discrepancies, similar to those found by Nagase et al. (1990), GFÖ, and DNB. This adds further weight to the argument that the Manchester & Peterson (1989) ephemeris is either erroneous or affected by timing noise; in a reanalysis of the Manchester & Peterson (1989) TOA data, DNB claim that there is evidence for a large glitch in the range MJD 46,900–47,000.

It is interesting to note that our frequency-based solution in Table 4 agrees with the local frequency measurements of both GFÖ and Ögelman & Hasinger (1990). The discrepancies all occur between our frequency-based solution and the long-term TOA-based solutions.[8] This fact may be explained if significant timing noise is present in the timing behavior of 0540−69. By way of comparison, for several pulsars with timing noise (i.e., 0832+26 and 0736−40, as discussed in Cordes & Downs 1985), the frequency residuals δf due to timing noise scale roughly as $\delta f \sim \delta\phi/T$, where T is the time span of monitoring, and $\delta\phi$ is the phase residual due to timing noise. Thus, over a timescale of ∼1–2 years, similar timing noise in 0540−69 could produce phase residuals of several cycles, clearly large enough to alter TOA-based solutions, while producing frequency modifications of only $\delta f \sim 10^{-7}$ Hz, too small to affect any of the frequency-based solutions we discuss here.

4.2. *TOA-determined Solutions*

We have seen above that we are able to fit successfully large subsections of the *ROSAT* TOA data set with smooth timing models of the form of equation 4. However, regardless of which pulsar position we assume and which subset of the TOAs we use to determine a preliminary solution, we are unable to produce a phase-coherent fit to the entire data set. This behavior strongly suggests the presence of timing noise that is contaminating the fits determined from the pulse TOAs. The presence of such noise in the timing behavior of pulsar 0540−69 may also explain the incompatibility of previous timing studies with one another, as some or all of them may have been contaminated by timing noise. While previous workers have suggested such a situation to explain their poor matches with other timing solutions, the incompatibilities have always been *between* different studies. Thus, there has always remained speculation that the observed incompatibilities are due to differences in analysis and handling of the data from one study to the next. However, this work has presented the first evidence of timing noise within a single self-contained study, and thus eliminates differences in the treatment of the data as a possible explanation for the timing discrepancies.

Solution O in Table 5, while only marginally unacceptable, gives a value for the braking index of $n \sim 2.5$, significantly different from previous determinations. Thus, even if we were to stretch our definition of a good fit, we would be left to conclude that the estimated braking index for 0540−69 varies with time. As Cordes & Downs (1985) note, such time variability is a prime indicator of the presence of timing noise.

Given that timing noise is present in the timing history of 0540−69, we would like to determine the form that such noise takes. Given a densely sampled timing data set, large discontinuities (glitches) would appear as "jumps" in the pulsar frequency and frequency derivative, with exponential recoveries. Even with somewhat sparser coverage, glitches typically leave long-term frequency-derivative offsets of $\Delta\dot{f}/\dot{f} \sim 10^{-4}$ (Lyne, Pritchard, & Smith 1993). However, the sparseness of our data set is so extreme, especially near TOAs 24–27, that we cannot determine $\dot{f}$ to sufficient accuracy to look for such an offset between the beginning and end of the data set.

[8] DNB use phase-coherent TOA analysis only over short time spans, due to clock problems with *Ginga*. See their paper for details.

Another form of timing noise would be smaller discontinuities, the so-called "random walk" timing noise (Cordes & Downs 1985). However, determining the characteristics of such timing noise can be very difficult even with a densely and evenly sampled timing data set. Given the uneven and sparse coverage of 0540−69 by *ROSAT*, we are unable to distinguish between large and small discontinuities, and thus we cannot hope to characterize the properties of any small discontinuities if they are present.

5. CONCLUSIONS

Using novel Fourier techniques, we have analyzed archival *ROSAT* observations of the Large Magellanic Cloud for a ∼3 yr time span in order to determine the timing characteristics of the young isolated pulsar 0540−69. We present the conclusions from this analysis below:

1. Using local frequency measurements, we determine a well-fitting timing solution with a braking index of $n = 2.5^{+0.6}_{-0.7}$. This timing solution is consistent with that of DNB, but is inconsistent with the TOA-based timing results of GFÖ, Ögelman, & Hasinger (1990), and Manchester & Peterson (1989).

2. Our frequency-based solution is consistent with the local frequency measurements of GFÖ and Ögelman & Hasinger (1990). This agreement may be understood in light of the discrepancy with their TOA-based solutions if timing noise similar to that seen in several other pulsars (e.g., Cordes & Downs 1985) is present in the timing behavior of 0540−69.

3. Using the frequency-based timing solution for 0540−69, we have constructed pulse profiles for the individual data segments and a master pulse profile. We find no evidence for time variability in the pulse shape over the 3 yr time span of the *ROSAT* observations.

4. Using the pulse profiles, we have determined pulse arrival times (TOAs) for 0540−69, and created TOA-based timing solutions. While we can successfully fit smooth spin-down models to subsets of the TOAs spanning up to ∼2 yr, we are unable to obtain acceptable phase-coherent fits to the entire 3 yr set of TOAs. This behavior indicates the presence of timing noise in 0540−69, and is the first evidence for such timing noise within a single, independent timing study.

5. The best-fitting TOA-based timing solution, using the pulsar position determined by DNB, is excluded at the 95% confidence level. Even accepting this solution, comparing its braking index ($n \sim 2.5$) to previous measurements would still require the presence of timing noise in 0540−69.

6. As a result of this timing noise, simple estimates of the braking index for 0540−69 using TOA analyses that ignore the timing noise are unreliable.

7. Given the sparseness and uneven sampling provided by the archival *ROSAT* coverage of 0540−69, we are unable to characterize the nature of this timing noise. Such work will require regular, frequent optical/X-ray observations of 0540−69 over a time span of several years.

We would like to thank the SAO PROS support group for help with the *ROSAT* data reduction and F. Seward, J. Cordes, R. Narayan, and J. Grindlay for helpful comments on an early draft of this work. S. E. was supported by a NASA Graduate Student Researcher Program fellowship through NASA Ames Research Center.

REFERENCES

Cordes, J. M., & Downs, G. S. 1985, ApJ, 59, 343
Deeter, J., Nagase, F., & Boynton, P. E. 1997, preprint
Eikenberry, S. S. 1997, Ph.D. thesis, Harvard Univ.
Eikenberry, S. S., Fazio, G. G., Ransom, S. M., Middleditch, J., Kristian, J., & Pennypacker, C. R. 1997, ApJ, 477, 465
Finley, J. P., Ögelman, H., Hasinger, G., & Trümper, J. 1993, ApJ, 410, 323
Gouiffes, C., Finley, J. P., & Ögelman, H. 1992, ApJ, 394, 581
Lyne, A. G., Pritchard, R. S., & Smith, F. G. 1993, MNRAS, 265, 1003
Manchester, R. N., Mar, D. P., Lyne, A. G., Kaspi, V. M., & Johnston, S. 1993, ApJ, 403, L29
Manchester, R. N., & Peterson, B. A. 1989, ApJ, 342, L23
Middleditch, J., & Pennypacker, C. R. 1985, Nature, 313, 659
Middleditch, J., Pennypacker, C. R., & Burns, M. S. 1987 ApJ, 315, 142
Nagase, F., Deeter, J., Lewis, W., Dotani, T., Makino, F., & Mitsuda, K. 1990, ApJ, 351, L13
Ögelman, H., & Hasinger, G. 1990, ApJ, 353, L21
Ransom, S. M., & Eikenberry, S. S. 1997, in preparation
Seward, F. D., Harnden, F. R., & Helfand, D. J. 1984, ApJ, 287, L19